BIOCHEMISTRY
including biophysical chemistry & molecular biology
Article

Biochemistry **2010,** *49,* 8455–8467 8455
DOI: 10.1021/bi101163u

Experimental Test of the Thermodynamic Model of Protein Cooperativity Using Temperature-Induced Unfolding of a Ubq−UIM Fusion Protein†

Mayank M. Patel,‡ Nikolaos G. Sgourakis,‡ Angel E. Garcia,§ and George I. Makhatadze*,‡

‡*Center for Biotechnology and Interdisciplinary Studies and Department of Biology and* §*Departments of Physics, Applied Physics, and Astronomy, Rensselaer Polytechnic Institute, 110 8th Street, Troy, New York 12065*

Received July 21, 2010; Revised Manuscript Received August 26, 2010

ABSTRACT: This study describes the thermodynamic characterization of a Ubq−UIM fusion construct (Ubq−UIM), designed from the ubiquitin−UIM interaction system, to determine whether it exhibits cooperativity of folding. The Ubq−UIM fusion constructs exhibit higher stability than the core Ubq molecule, consistent with the finding that the UIM helix is docked to Ubq. Temperature-induced unfolding profiles of Ubq−UIM were monitored by DSC and far-UV and near-UV CD spectroscopies. Ubq−UIM appears to exhibit cooperative unfolding as indicated by results of global fits of a two-state model to far- and near-UV CD and DSC thermal unfolding data. The cooperativity of Ubq−UIM unfolding was further tested by the amino acid substitutions that selectively stabilize or destabilize Ubq, UIM, and/or the interface. The effects of these substitutions on the thermodynamic properties of Ubq−UIM are described well by a thermodynamic model for cooperativity in proteins. In particular, a substitution that lowered the stability of the Ubq−UIM interface indeed led to a decrease in cooperativity.

The question of cooperativity is of paramount interest in the field of protein folding. Depending on native topology, single-domain proteins can exhibit a two-state (*1*, *2*) or multistate folding behavior (*3*). Multidomain proteins are more likely to follow a noncooperative unfolding pathway, wherein the individual domains are intrinsically stable and able to fold and unfold independently with respect to one another, followed by their coalescence to form the native structure (*4*−*10*). This is generally manifested in stabilization of an intermediate state, the detection of which is used to determine noncooperativity of folding (*11*−*13*). Arguably, a defining difference between two-state and multistate unfolding behavior is established by the relative magnitudes of stability of independently foldable subunits and stability of interactions between such subunits in a protein. Weak interactions between subunits increase the difference between secondary and tertiary structure stability, leading to deviations from folding cooperativity (*14*). In this case, properties of the native protein molecule can be deduced from a sum of the properties of its various subunits (*15*, *16*). Alternatively, larger proteins can exhibit folding cooperativity if extensive stabilizing interactions are present between subunits (*17*−*20*).

Protein engineering has been proven to be a valuable tool for investigating cooperativity in protein folding. Some studies have adopted the protein dissection approach, monitoring stabilities of individual subunits, to parse cooperativity in protein folding (*10*, *21*−*24*), while others have designed fusion proteins either by swapping subunits between homologous proteins (*25*) or by linking two molecules of the same protein (*9*). In the absence of a stabilizing interface between the linked molecules, a conversion from two-state to multistate folding behavior is observed upon their covalent linkage (*9*, *17*, *18*, *25*). Also, a switch from cooperative to noncooperative unfolding behavior of the three-helix spectrin domains was observed upon introduction of decoupling mutations (*26*). These reports reinforce the notion that affinity between subunits can be critical for folding cooperativity in proteins, stressing the importance of investigating the thermodynamic basis of interactions between subunits in proteins.

The ubiquitin−ubiquitin interacting motif (UIM) interaction system provides an appealing paradigm for addressing this need. This interaction forms the underlying basis for endosomal sorting and lysosomal degradation of monoubiquitinated membrane proteins (*27*−*31*). Specific targeting to the cellular destination depends on ubiquitin recognition by numerous ubiquitin binding domains (UBD) within proteins in the endocytic pathway. The ubiquitin interacting motif (UIM) is a prevalent class of UBD and comprises a short, approximately 20-residue, structural element comprised of a highly conserved e-e-e-e-Φ-X-X-A-Φ-X-Φ/e-S-X-X-e core, where e is an acidic residue, Φ represents a large hydrophobic residue, and X can be any residue (*32*, *33*). In general, UIMs from various proteins bind to ubiquitin with low affinities (K_d values in the high micromolar to millimolar range) (*31*, *34*−*36*). Structural studies have demonstrated that UIM peptides form amphipathic helices and bind with a 1:1 stoichiometry to Ubq using the highly conserved, hydrophobic L8-I44-V70 (L17-I53-V79 in our construct) surface of the latter (*36*−*40*). In addition, electrostatic interactions between R42 and R72 (R51 and R81 in our construct) in Ubq and acidic residues at the N-terminus of UIMs are crucial for complex formation (*37*, *40*).

One prominent example of a UIM-harboring protein involved in endocytotic protein sorting is VPS27p from *Saccharomyces cerevisiae* (*32*, *41*). Structures of Ubq−VpsUIM complexes show that this UIM is highly helical and the modes of interaction between the two molecules are very similar to those for other

†This work was supported by the National Institutes of Health (Grant R01-GM054537).

*To whom correspondence should be addressed: Center for Biotechnology and Interdisciplinary Studies, Rensselaer Polytechnic Institute, 110 8th St., Troy, NY 12180. Phone: (518) 276-4417. Fax: (518) 276-2955. E-mail: makhag@rpi.edu.

Published on Web 09/13/2010

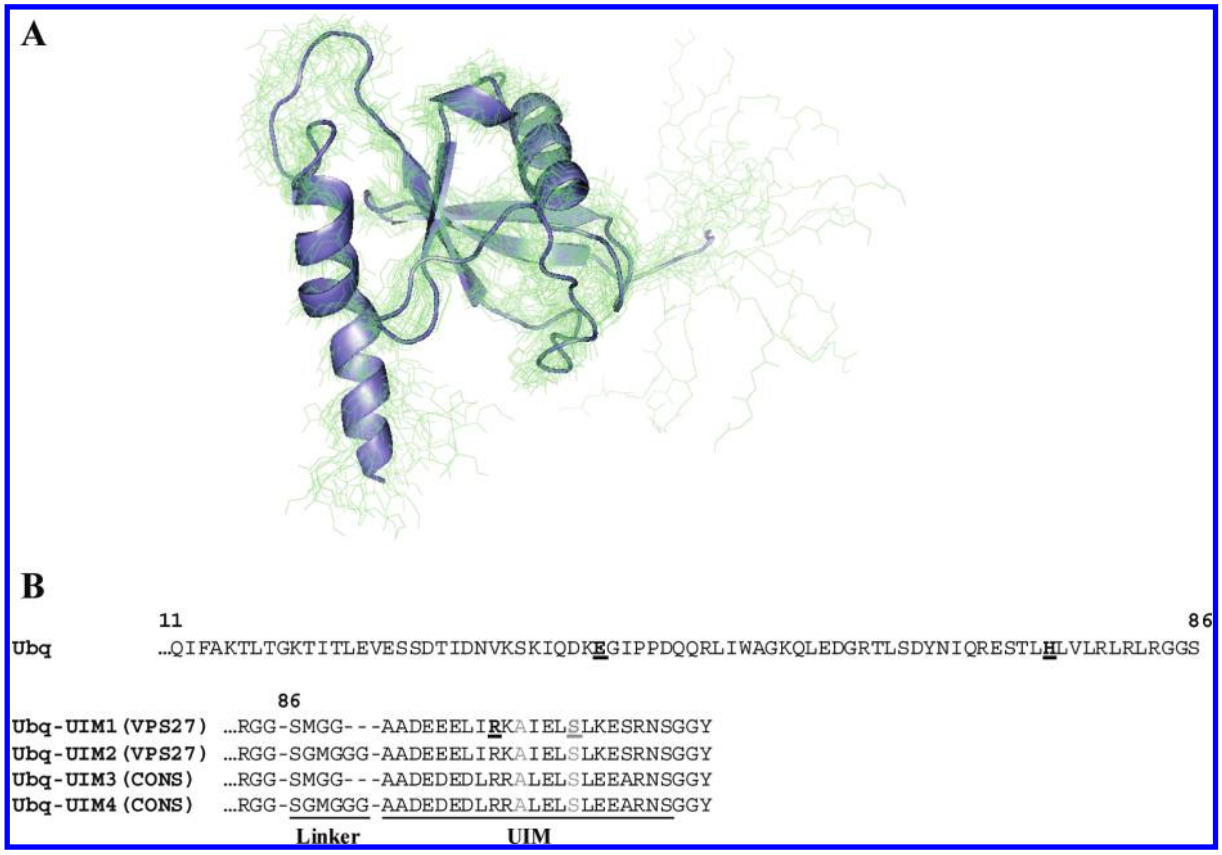

FIGURE 1: (A) Cartoon representation of the three-dimensional structure of the Ubq−UIM fusion construct determined by NMR spectroscopy [Protein Data Bank entry 2KDI (*42*)]. Main chain conformations for the 20 lowest-energy structures are colored green, and the calculated average structure is shown as a blue ribbon. (B) Sequence alignment of Ubq and four Ubq−UIM fusion constructs. Bold and underlined letters show the sites of mutation. The Ala and Ser residues in the UIM helix highlighted in gray are 100% conserved and define a crucial part of the -X-A-ϕ-X-ϕ/e-S- motif that enables binding of all UIM sequences to Ubq.

UIMs as described above (*36*, *37*). Additionally, the orientation of the UIM helix in the Ubq−UIM complex closely juxtaposes the C-terminus of Ubq and N-terminus of UIM. We have utilized this proximity to introduce a flexible linker between the two molecules to generate a fusion construct (Ubq−UIM) and determined its structure using NMR spectroscopy (*42*). This structure establishes that the common hydrophobic interface between Ubq and UIM, centered around the I44 (I53 in our construct) patch of Ubq, is preserved in the Ubq−UIM fusion construct (Figure 1A). A parallel characterization of the secondary structure and thermodynamic stability of the Ubq−UIM fusion protein and of unlinked Ubq and UIM provides an optimal opportunity for advancing our understanding of the relationship between intra- and intersubunit stability and folding cooperativity in proteins. Specifically, we have tested the potential of the Ubq−UIM fusion construct in studying protein folding in terms of the relationship between the stability of isolated α-helices and those in larger or multidomain proteins.

This study describes the structural and thermodynamic characterization of four Ubq−UIM constructs differing in UIM sequence and linker length. We have previously determined the high-resolution structure of one of the Ubq−UIM fusion constructs using NMR spectroscopy, which confirmed the docked state of the UIM helix and the location of the binding interface on Ubq (*42*). Analysis of temperature-induced unfolding profiles, monitored by far- and near-UV circular dichroism (CD) and differential scanning calorimetry (DSC), reveals that the fusion proteins are more stable than Ubq by ~10 °C, consistent with the docked state of the UIM helix on Ubq in the fusion constructs. Both CD and DSC temperature-induced melting profiles show a single transition and could be globally fitted to a two-state model, indicating that the fusion proteins exhibit cooperativity upon thermal unfolding. We have further tested the cooperativity of Ubq−UIM protein unfolding by rationally introducing amino acid substitutions that selectively stabilize or destabilize Ubq, UIM, and/or the interface. The effects of these substitutions on the thermodynamic properties are described well by a thermodynamic model for cooperativity in proteins.

MATERIALS AND METHODS

Cloning, Expression, and Purification. PCR step mutagenesis was conducted on cDNA encoding yeast ubiquitin with an N-terminal six-His tag to generate a V5A/F45W variant (*43*, *44*) of Ubq. This DNA sequence was extended at the C-terminus by multiple primer extension steps to link the coding sequence of the yeast VPS27 N-terminal ubiquitin-interacting motif (UIM), corresponding to residues 258−279 of VPS27, to generate a gene encoding a covalently linked Ubq−UIM fusion construct. Two such genes were constructed that differed in the length of the linker region between Ubq and UIM: four (Ubq-SMGG-UIM) and six (Ubq-SGMGGG-UIM) residues (Figure 1). These will be termed Ubq−UIM1 and Ubq−UIM2, respectively. Two additional genes encoding fusion constructs containing a consensus UIM sequence (see below) were also constructed with same linker residues. These will be termed Ubq−UIM3 (four linker residues) and Ubq−UIM4 (six linker residues). A tyrosine residue separated by two glycine residues was also added to the C-terminus of

all UIM sequences. The coding sequences for Ubq and all Ubq−UIM constructs were subcloned into the pGia expression vector (*45*) using standard molecular biology protocols. Mutations were introduced into Ubq and Ubq−UIM1 plasmids using the QuikChange site-directed mutagenesis kit from Stratagene.

Overexpression of the cloned proteins was achieved by transformation of the corresponding plasmid constructs into *Escherichia coli* strain BL21(DE3)pLysS, followed by growth in 2xYT medium to an optical density of 1.1−1.5 at 600 nm. Protein expression was induced by the addition of 1 mM IPTG. Cells were incubated for an additional 2−3 h, harvested by centrifugation at 4000 rpm, and resuspended in 100 mM sodium phosphate and 10 mM Tris-HCl buffer (pH 8.5) containing 8 M urea. Proteins were purified from cell lysate using Ni-NTA resin (Novagen) under denaturing conditions, as recommended by the resin manufacturer. The second purification step included gel-filtration chromatography on a Sephadex G-75 (Amersham Pharmacia) column (2.5 cm × 100 cm) in 5% acetic acid. As the final purification step, reverse-phase HPLC (Waters Corp.) on a C18 column and a 0 to 100% acetonitrile gradient in the presence of 0.065−0.05% TFA was employed. Protein yields ranged from 40 to 60 mg/L of bacterial culture. The purity of the resulting protein preparations was better than 95%, as judged by the Coomassie staining of SDS−polyacrylamide gels.

The VPS27 UIM peptides GAADEEELIRKAIELSLKESRNSGGY and GAADEEELIVKAIELSLKESRNSGGY (difference in sequence underlined) were synthesized at The Pennsylvania State University College of Medicine Core Facility, by solid-phase procedures on a Milligen 9050 FMoc peptide synthesizer. Peptides were purified via reverse-phase HPLC using a C18 column and a 0 to 100% acetonitrile gradient in the presence of 0.065−0.05% TFA. The resulting fractions containing peptide were pooled, lyophilized, and resuspended in deionized water. The process was repeated twice to remove residual TFA. Peptides were finally lyophilized and stored under dry conditions at −20 °C. The purity and identity of the recombinant proteins and UIM peptide were confirmed by MALDI-TOF mass spectroscopy. Protein and peptide concentrations were determined spectrophotometrically using the following extinction coefficients: $\varepsilon_{280} = 6990\ M^{-1}\ cm^{-1}$ for Ubq, $\varepsilon_{280} = 8480\ M^{-1}\ cm^{-1}$ for Ubq−UIM proteins, and $\varepsilon_{280} = 1490\ M^{-1}\ cm^{-1}$ for the UIM peptide (*46*).

Consensus Sequence for the Ubiquitin Interacting Motif (UIM). A multiple-sequence alignment of 670 UIM sequences from the pfam database (*47*) was used to determine positional frequencies of each residue in the sequence using the following relationship:

$$\psi = \frac{\dfrac{N_i(\mathrm{x})}{\text{no. of sequences}}}{\dfrac{\sum N_i(\mathrm{x})}{\text{total no. of sequences}}} \quad (1)$$

where N_i(x) is the number of times residue x appears at position *i*. To eliminate intrinsic UIM sequence bias, the consensus residue was required to have a ψ value at least 2 times larger than its frequency in all of the pfam database. The final consensus sequence (GAADEDEDLRRALELSLEEARNSGGY) was used to generate two Ubq−UIM fusion proteins (Ubq−UIM3 and Ubq−UIM4) with different linker lengths, as described above.

Sedimentation Equilibrium. To evaluate the possibility of oligomerization in all proteins, equilibrium analytical ultracentrifugation experiments were performed. All measurements were taken on a Beckman XLA analytical ultracentrifuge. Two concentrations for all proteins, 7 and 21 μM, were analyzed at pH 7.4 by monitoring the absorbance at 280 nm in six-sector cells. Samples were equilibrated at three rotor speeds (18000, 25000, and 32000 rpm). Absorbance data were fitted to a single-species model described by the following equation:

$$A(r) = I_o + C_m(r_o)\exp\left[\frac{M_m(1-\rho\bar{V})\omega^2(r^2-r_o{}^2)}{2RT}\right] \quad (2)$$

where $A(r)$ is the absorbance at radial position r, M_m is the molecular mass of the protein, $\bar{V}$ is the partial specific volume of the protein, calculated from the amino acid composition (*48*), ρ is the solution density, I_o is the baseline offset term, and ω is the rotor angular velocity. Data were analyzed using the nonlinear regression routine NLREG and in-house written scripts (*45*).

Circular Dichroism. CD experiments were conducted on a JASCO J-715 spectropolarimeter. Far-UV and near-UV CD spectra were recorded in triplicate at 22 °C in 1 mm or 1 cm quartz cylindrical cuvettes at concentrations of 0.3 and 1 mg/mL, respectively. All experiments were conducted in CD buffer containing sodium borate, sodium citrate, and sodium phosphate (1 mM each) (*49*, *50*). The signal is expressed as mean residue ellipticity [Θ] (degrees square centimeters per decimole).

Thermal unfolding profiles of all proteins were monitored by changes in ellipticity at 222 nm as a function of temperature. Temperature was controlled with either a Neslab automated circulating water bath for a 1 mm water-jacketed cylindrical quartz cuvette or a six-position Peltier effect cell changer for a 1 cm rectangular quartz cuvette. Ellipticity values as a function of temperature were fitted to a two-state model:

$$\theta(T) = F_N(T)\theta_N(T) + F_U(T)\theta_U(T) \quad (3)$$

where $\theta(T)$ is the measured ellipticity at any given temperature, $\theta_N(T)$ and $\theta_U(T)$ are the ellipticity values of the native and unfolded protein at this temperature, respectively, and F_N and F_U are the fractions of the native and unfolded protein at this temperature, respectively. Fractions of the native and unfolded proteins were calculated as

$$F_N(T) = 1 - F_U(T) = \frac{1}{1+K(T)} \quad (4)$$

where K is the equilibrium constant of the two-state unfolding reaction calculated as

$$K(T) = e^{-\Delta G(T)/RT} \quad (5)$$

ΔG of the unfolding reaction was calculated as

$$\Delta G(T) = (T_m - T)\left[\frac{\Delta H(T_m)}{T_m} - \Delta C_p\right] - T\Delta C_p \ln\left(\frac{T}{T_m}\right) \quad (6)$$

where T_m is the transition temperature, $\Delta H(T_m)$ is the enthalpy change at the transition temperature, ΔC_p is the heat capacity change upon unfolding, assumed to be temperature-independent.

The ellipticities of a fully helical peptide ($[\Theta]_H$) and fully coiled peptide ($[\Theta]_C$) of a given number of residues (N_r) at a given temperature (T) were calculated from the following equations (*51*)

$$[\Theta]_H = (-40000 + 250T)\left(1 - \frac{2.5}{N_r}\right) \quad (7)$$

$$[\Theta]_C = 640 - 45T \quad (8)$$

The difference in the helical content of the UIM peptide between the fusion protein and unbound forms was determined by

$$\Delta[\Theta]_{222} = \frac{\Theta_{\mathrm{Ubq-UIM}} - \Theta_{\mathrm{Ubq}}}{N_{\mathrm{UIM}}} \quad (9)$$

where $\Theta_{\mathrm{Ubq-UIM}} - \Theta_{\mathrm{Ubq}}$ is the difference in the molar ellipticities of the two proteins and N_{UIM} is the number of residues in the UIM peptide.

Differential Scanning Calorimetry. DSC experiments with Ubq and all Ubq−UIM proteins were conducted on a VP-DSC instrument (Microcal Inc., Northampton, MA) at a scan rate of 90 deg/h. Protein concentrations were ~2 mg/mL in 20 mM sodium phosphate (pH 7.4). The reversibility of unfolding was checked by recording the second scan, which was found to be more than 90% as judged by the area under the excess heat capacity function. Calorimetric profiles were analyzed using nonlinear regression routine NLREG and scripts written in-house. Thermodynamic functions under reference conditions were calculated as

$$\Delta H(T) = \Delta H(T_{\mathrm{m}}) + \Delta C_p(T - T_{\mathrm{m}}) \quad (10)$$

$$\Delta S(T) = \Delta S(T_{\mathrm{m}}) + \Delta C_p \ln\left(\frac{T}{T_{\mathrm{m}}}\right) = \frac{\Delta H(T_{\mathrm{m}})}{T_{\mathrm{m}}} + \Delta C_p \ln\left(\frac{T}{T_{\mathrm{m}}}\right) \quad (11)$$

$$\Delta G(T) = \Delta H(T) - T\Delta S(T) \quad (12)$$

where $\Delta H(T)$, $\Delta S(T)$, and $\Delta G(T)$ are the enthalpy, entropy, and Gibbs free energy functions of a protein, respectively. ΔC_p is the heat capacity change upon protein unfolding.

The ΔC_p values for Ubq and Ubq−UIM constructs were determined from its relationship with the change in water accessible surface area (ΔASA) of a protein upon unfolding, using the following parametrization (*52*):

$$\Delta C_p = 2.14\Delta\mathrm{ASA}_{\mathrm{aliph}} + 1.55\Delta\mathrm{ASA}_{\mathrm{arom}} - 1.81\Delta\mathrm{ASA}_{\mathrm{peptide}} - 0.88\Delta\mathrm{ASA}_{\mathrm{polar}} \quad (13)$$

where the ΔASA terms for aliphatic (aliph), aromatic (arom), protein backbone (peptide), and polar (polar) residues were calculated as described previously (*53*). For calculation of the ASA of the folded state, the three-dimensional structures of the proteins were used [PDB entry 2KDI for Ubq−UIM (*42*)], and the structure of the core Ubq molecule was generated by deleting linker and UIM residues. The unfolded state structure was modeled as an extended chain with the same amino acid sequence. The calculated value of ΔC_p for Ubq (3.1 kJ mol^{-1} K^{-1}) is in excellent agreement with the experimental value (3.2 kJ mol^{-1} K^{-1}) determined previously (*54*). Such agreement warrants the use of the calculated value of ΔC_p for the Ubq−UIM construct. Furthermore, this value agrees well with the value determined from the actual calorimetric profiles as a difference between partial molar heat capacities of the native and unfolded states.

Fluorescence Anisotropy. The UIM peptide was labeled with Alexa Fluor 488 (protein labeling kit) from Molecular Probes/Invitrogen according to the manufacturer's specifications. Briefly, 50 μL of 0.1 M sodium bicarbonate was added to 0.5 mL of 2 mg/mL peptide. The peptide solution was then mixed with the reactive dye. The reaction continued for 1 h at room temperature, while the mixture was slowly stirred and protected from the light. The separation of the labeled protein from the free dye was accomplished using a Sephadex G-10 column.

Anisotropy experiments were performed with a Fluoromax spectrofluorimeter at 25 °C. The sample was excited with perpendicularly polarized light, and the vertical and horizontal components were recorded (I_{VV} and I_{VH}, respectively). To calculate the G factor, the sample was excited with horizontally polarized light and the vertical and horizontal components were recorded (I_{HV} and I_{HH}, respectively). The excitation and emission wavelengths were 494 and 519 nm, respectively, and the anisotropy values were calculated according to the following equation:

$$r = \frac{I_{\mathrm{VV}} - GI_{\mathrm{VH}}}{I_{\mathrm{VV}} + 2GI_{\mathrm{VH}}} \quad (14)$$

where G was calculated as

$$G = \frac{I_{\mathrm{HV}}}{I_{\mathrm{HH}}} \quad (15)$$

The binding isotherm was analyzed as

$$r = \left[[\mathrm{UIM}]_{\mathrm{T}} + [\mathrm{Ubq}] + 1/K - \sqrt{([\mathrm{UIM}]_{\mathrm{T}} + [\mathrm{Ubq}] + 1/K)^2 - 4[\mathrm{UIM}]_{\mathrm{T}}[\mathrm{Ubq}]}\right]/(2[\mathrm{UIM}]_{\mathrm{T}}) \quad (16)$$

where $[\mathrm{UIM}]_{\mathrm{T}}$ is the total concentration of UIM in the experiment, [Ubq] is the concentration of ubiquitin, and K_{d} is the equilibrium constant.

Molecular Dynamics Simulations. The NMR structural ensemble of the Ubq−UIM protein, previously reported by our group (*42*), was used as a starting point in all simulations. The fully solvated protein systems were constructed from the 20 lowest-energy structures of the NMR ensemble in the following manner. Each system was subjected to a short energy minimization using the steepest descent algorithm. The protein was then solvated using 9792 water molecules in a cubic box. The addition of three sodium ions ensured charge neutrality of the system. Following another energy minimization step, the solvated system was brought to a final temperature of 550 K in three equilibration steps of 50 ps each at 100, 300, and 550 K. At this stage, the use of the Berendsen (*55*) thermostat under constant-volume conditions enabled rapid convergence to the desired temperature. The pressure of each system was then equilibrated to 200 atm using 100 ps of constant-pressure simulations with the Berendsen barostat (*55*). This resulted in final dimensions of the solvated systems of approximately 74 Å × 74 Å × 74 Å. For each system, we performed 10 ns of molecular dynamics under the NPT ensemble, at 200 atm. At this stage, we used the Parrinello−Rahman (*56*) pressure control with a 5 ps relaxation time and a compressibility of 4.6×10^{-5} atm^{-1}, and the Nose-Hoover temperature coupling (*57*, *58*). The pressure was chosen such that water was in the liquid phase at this temperature. At this stage, the use of the LINCS (*59*) and settle (*60*) algorithms to constraint high-frequency bond vibrations allowed the use of a 2 ps integration step. For all simulations, the FF99SB force field (*61*) and Tip4p-Ew water model (*62*) were used. The electrostatic interactions were treated by the smooth particle mesh

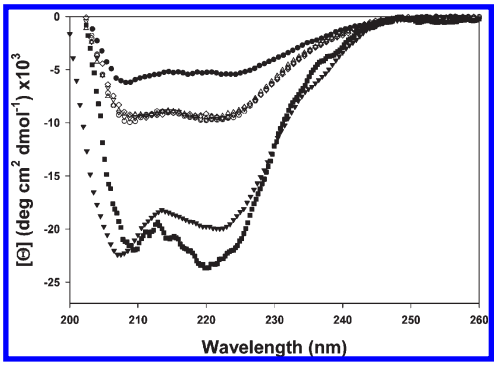

FIGURE 2: Far-UV circular dichroism spectra of Ubq core (●), VPS27 UIM peptide (▼), and all Ubq−UIM fusion constructs: Ubq−UIM1 (○), Ubq−UIM2 (▽), Ubq−UIM3 (△), and Ubq−UIM4 (◇). The difference spectrum between Ubq−UIM and Ubq calculated from eq 9 is shown as solid squares (■). For the sake of clarity, only every tenth data point is shown in all spectra.

Ewald (PME) method (*63*), using a 75 × 75 × 75 grid, with fourth-order charge interpolation and a real space cutoff of 1.0 nm. The Ewald Gaussian width ($1/\beta$) is 0.320 nm, corresponding to a relative accuracy of the Ewald sum of 10^{-5}. The GROMACS simulation engine was used (*64*) on a Linux-based cluster.

RESULTS AND DISCUSSION

Fusion Constructs Are Monomeric in Solution−Sedimentation Equilibrium. The main objectives of this study are to characterize the thermodynamic stabilities of the Ubq−UIM fusion constructs and to determine whether they exhibit a two-state unfolding behavior. A possibility exists that in the covalently linked constructs, the UIM helix from one Ubq−UIM molecule could dock on to the Ubq core of a second Ubq−UIM molecule. This would manifest itself in the form of noncovalent "swapped" dimers (*65*). To evaluate the possibility of oligomerization, sedimentation equilibrium experiments were conducted at pH 7.4. The fusion constructs were found to be monomeric over the concentration range used in the experiments (see Figure S1 of the Supporting Information).

Secondary Structure Characterization of UIM and the Ubq−UIM Construct. The far-UV CD spectrum of the VPS27 UIM peptide is shown in Figure 2. It is clear that the unbound peptide is very helical; comparison with the calculated mean residue ellipticity for fully helical and fully coiled peptides of the same length at 25 °C (eqs 7 and 8) yields a helical content of ~57% for the UIM peptide.

Similarly, all four Ubq−UIM fusion constructs show that these proteins contain a large fraction of helical structure as judged from the comparison with the far-UV CD spectrum of the Ubq core (Figure 2). To determine whether binding to Ubq is coupled to a change in UIM helical content, the ellipticity of the UIM peptide alone was compared with the UIM ellipticity in the fusion construct. Because all fusion constructs exhibit very similar far-UV CD spectra, the change in UIM helical content upon docking to Ubq was determined by the normalized difference in the CD spectra of Ubq−UIM1 and Ubq (eq 9). The resulting difference spectrum shown in Figure 2 clearly indicates a further increase in the helical content of UIM by ~10% in the fusion construct (assuming that all changes in ellipticity originate from UIM). Combined with the strong structural evidence that the UIM helix is docked to Ubq in the fusion construct (*42*), this observation suggests that the Ubq−UIM binding event is coupled to some conformational changes in UIM.

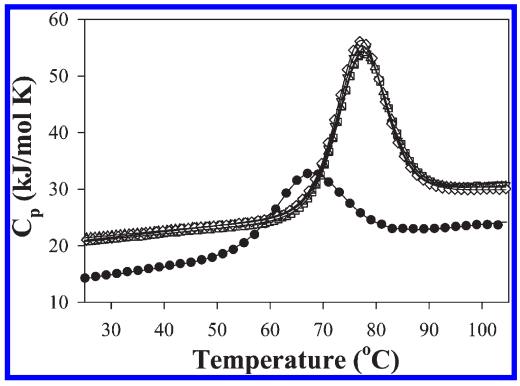

FIGURE 3: Temperature dependence of the partial molar heat capacity of the Ubq core and Ubq−UIM fusion constructs as monitored by DSC. Symbols show, for the sake of clarity, every third experimental data point: (●) ubiquitin core, (○) Ubq−UIM1, (□) Ubq−UIM2, (△) Ubq−UIM3, and (▽) Ubiq−UIM4. Solid lines represent the fit to a two-state model.

Ubq−UIM Stability and Ubq−UIM Binding Affinity. An expected outcome of docking of the UIM helix to Ubq would be an increase in the stability of the Ubq−UIM construct over that of Ubq. Indeed, comparison of the melting profiles of Ubq and all fusion proteins, determined from DSC experiments (Figure 3), shows that the transition temperatures of all fusion constructs are higher than that of the Ubq core by at least 10 °C. Also, the T_m and $\Delta H(T_m)$ values among all fusion proteins are remarkably similar (Table 1). This agreement in conformational stabilities of all Ubq−UIM constructs indicates that (1) the consensus sequence is comparable to that of VPS27 UIM in its ability to bind Ubq and enhance the stability of the fusion protein (compare Ubq−UIM1 and Ubq−UIM2 with Ubq−UIM3 and Ubq−UIM4) and (2) there is no detectable dependence of Ubq−UIM structure and stability on the linker lengths used in these experiments (compare Ubq−UIM1 and Ubq−UIM3 with Ubq−UIM2 and Ubq−UIM4); i.e., the linker is sufficiently long and does not impose strain. This is discussed in more detail below.

The free energies of unfolding (ΔG) of all proteins, determined from eqs 10−12, show that all fusion constructs are more stable than Ubq by 15 ± 1 kJ/mol (Table 1). This extent of stabilization, determined as the difference in Gibbs free energies of unfolding of the Ubq−UIM fusion protein and Ubq ($\Delta G_{Ubq-UIM} - \Delta G_{Ubq}$) at 25 °C, essentially provides a measure of the binding free energy, which yields an apparent dissociation constant ($K_{d,intra}$) of 2.1 ± 0.1 mM, of UIM to Ubq in the context of the covalently linked fusion construct.

To determine the effect of covalent linkage on Ubq−UIM binding affinity, we need to compare $K_{d,intra}$ with the dissociation constant for binding of free UIM to Ubq ($K_{d,inter}$). $K_{d,inter}$ was determined using a fluorescence anisotropy experiment with the core Ubq molecule and fluorescently labeled UIM peptide (Figure 4). Analysis of the binding isotherm with a model with 1:1 stoichiometry provides a $K_{d,inter}$ of 0.09 ± 0.01 mM. This value compares well with the values obtained using other techniques such as NMR and SPR [0.2−0.3 mM (*36*, *37*)] and suggests that Ubq−UIM binding affinity becomes weaker by at least 1 order of magnitude upon covalent linkage of the two molecules. This outcome seems contrary to intuition because covalent linkage of two molecules would be expected to increase the local concentration of the ligand (UIM). However, precedence for our observation exists in other systems, e.g., destabilization of covalently linked subunits that otherwise form noncovalent

Table 1: Thermodynamic Parameters of Ubq and Ubq−UIM Fusion Proteins at pH 7.4

	T_m (°C)	$\Delta H(T_m)$ (kJ/mol)	ΔC_p (kJ mol^{-1} K^{-1})	ΔH(25 °C) (kJ/mol)	ΔG(25 °C) (kJ/mol)
Ubq[a]	66 ± 1	215 ± 2	3.1	88 ± 2	18 ± 2
Ubq−UIM1[a]	77 ± 1	329 ± 2	4.0	121 ± 2	33 ± 1
Ubq−UIM2[a]	77 ± 1	330 ± 3	4.0	122 ± 3	33 ± 1
Ubq−UIM3[a]	77 ± 1	335 ± 4	4.0	127 ± 4	34 ± 1
Ubq−UIM4[a]	77 ± 1	334 ± 3	4.0	126 ± 3	33 ± 1
H77 V_Ubq−UIM[a]	84 ± 1	340 ± 3	4.0	100 ± 3	36 ± 1
E43N_Ubq−UIM[a]	70 ± 1	298 ± 4	4.0	118 ± 4	27 ± 2
S104A_Ubq−UIM[b]	68 ± 1	225 ± 4	4.0	53 ± 3	17 ± 1
R98 V_Ubq−UIM[c]	73 ± 1	301 ± 3	4.0	109 ± 3	28 ± 1

[a]Obtained from global fits of DSC and far- and near-UV CD. [b]Obtained from global fits of DSC and near-UV CD. [c]Obtained from global fits of far- and near-UV CD thermal melting profiles to a two-state unfolding model. The corresponding thermal melting profiles are shown in Figures 3, 5, and 7. ΔH(25 °C) and ΔG(25 °C) were determined from eqs 10 and 12, respectively, using ΔC_p values determined from eq 13.

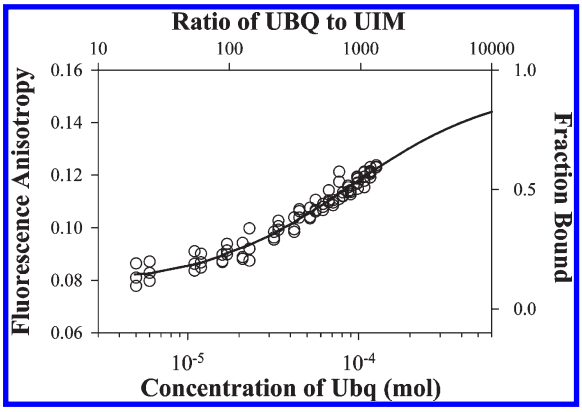

FIGURE 4: Binding isotherm of the Ubq core and VPS27 UIM peptide as monitored by changes in the fluorescence anisotropy of the labeled peptide (see Materials and Methods for details). The solid line is the experimental data fit to eq 16 with a $K_{d,inter}$ of 0.09 ± 0.01 mM.

dimers in the wild-type protein (*66*−*68*). Several detailed studies of this effect revealed that it is related to the entropy loss due to loop formation (*68*−*70*). On the basis of these results combined with the estimates for the translation entropy changes upon protein association (*71*, *72*), the expected decrease in the binding energy due to the loss of entropy is on the order of 5−7 kJ/mol for the loop length in Ubq−UIM constructs (six to eight residues). This value compares well with the experimentally observed decrease in the apparent ΔG of binding of 7 ± 1 kJ/mol (calculated from the difference between $K_{d,inter}$ and $K_{d,intra}$).

Cooperativity of Ubq−UIM Fusion Constructs. The major goal of this study serves to explore whether the Ubq−UIM fusion protein exhibits a two-state or multistate unfolding behavior. To address this, we have compared thermal stability profiles as followed by spectroscopic and calorimetric techniques, because this correlation has been traditionally used to determine cooperativity in protein folding (see, e.g., refs (*73*−*77*)). The rationale behind comparing unfolding data from different techniques is that they are able to monitor structural changes at different levels. The far-UV CD signal reports on the secondary structure content of proteins. Although the far-UV CD signal at 222 nm in the Ubq−UIM construct is dominated by the UIM helix, the 10-residue helix in the Ubq core also contributes to this signal (Figure 2), meaning that this technique provides information about changes in helical content in the Ubq−UIM construct. On the other hand, unfolding profiles obtained from the CD signal at 260 nm, i.e., in the near-UV CD region, arise from chromophores in aromatic residues, which are sensitive to changes

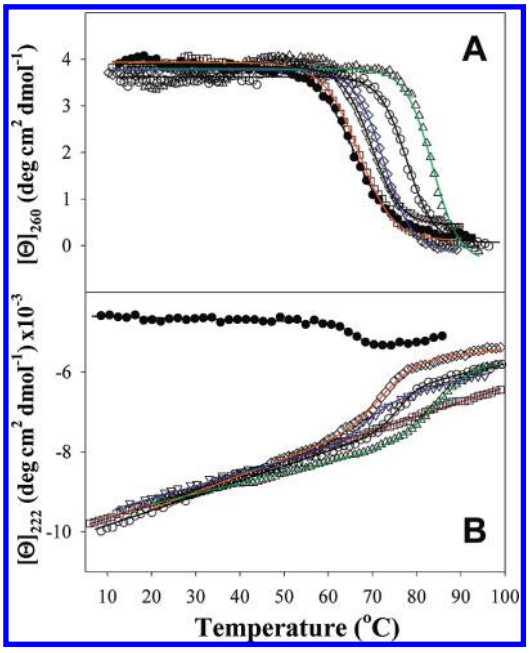

FIGURE 5: (A) Temperature-induced melting profiles of the Ubq core and Ubq−UIM construct variants monitored by changes in near-UV CD ellipticity at 260 nm. (B) Temperature-induced melting profiles of the Ubq core and Ubq−UIM construct variants monitored by changes in far-UV CD ellipticity at 222 nm. The solid red line in panel B drawn through the experimental data points for S104A_Ubq−UIM is simply to guide the eye. Symbols for both panels are experimental data: (●) ubiquitin core, (○) Ubq−UIM, (□) S104A_Ubq−UIM, (△) H77V_Ubq−UIM, (▽) E43N_Ubq−UIM, (◇) R98V_Ubq−UIM. Solid lines represent the fit to a two-state model (Ubq and Ubq−UIM, black; H77V_Ubq−UIM, green; S104A_Ubq−UIM, red; E43N_Ubq−UIM, blue; R98V_Ubq−UIM, orange).

in overall tertiary structure. Thus, near-UV CD will largely report on the conformational changes within the Ubq core. Finally, DSC provides a direct measurement of the overall thermodynamic stability of the molecule. Thus, an overlap between the thermal melting profiles determined from these techniques would mean that upon temperature-induced unfolding different elements of protein structure are lost simultaneously, which provides evidence that a protein unfolds cooperatively.

Temperature-induced unfolding profiles of the Ubq−UIM1 protein as monitored by far- and near-UV CD are shown in Figure 5. For comparison, the unfolding profiles of Ubq are shown. As in the case of DSC (Figure 3), the Ubq−UIM1 protein shows a markedly higher transition temperature. Furthermore, the CD-monitored thermal unfolding curves for both Ubq and

the Ubq−UIM1 construct appear to show a single sigmoidal transition. These profiles were analyzed according to a two-state model together with the DSC profiles using common thermodynamic parameters, T_m, $\Delta H(T_m)$, and ΔC_p, as described by eqs 10−12. All three (far- and near-UV CD and DSC) unfolding profiles for Ubq, a protein with well-established two-state unfolding behavior (*43*), can be described well by a global two-state unfolding model (see Materials and Methods). Importantly, the unfolding profiles for the Ubq−UIM1 construct monitored by all three different methods can also be fit to a two-state model with common thermodynamic parameters (see Figures 3 and 5 for the quality of the fits and Table 1 for the fitted parameters). On the basis of these observations, we can conclude that all Ubq−UIM proteins appear to undergo two-state (cooperative) temperature-induced unfolding.

Effects of Selective Modulation of Ubq, UIM, and/or Interface Stability. The results presented above suggest that temperature-induced unfolding of Ubq−UIM constructs closely follows a cooperative all-or-none unfolding. This is based on the observations that the melting profiles monitored by far- and near-UV CD spectroscopy and by DSC can be fit by a two-state model using a common set of thermodynamic parameters. The cooperative behavior of the Ubq−UIM1 protein variant, because all four Ubq−UIM constructs show the same behavior, was examined in more detail. We tested the cooperativity of this fusion construct (hereafter we will call Ubq−UIM1 and VPS27 UIM simply Ubq−UIM and UIM, respectively) by rationally introducing amino acid substitutions into Ubq−UIM that selectively stabilize or destabilize the Ubq core, the UIM helix, and/or the Ubq−UIM interface. This approach is based on a thermodynamic model of protein cooperativity, in which the stability of Ubq−UIM can be represented as (*78*−*81*)

$$\Delta G_{\mathrm{Ubq-UIM}}(T) = \Delta G_{\mathrm{Ubq}}(T) + \Delta G_{\mathrm{UIM}}(T) + \Delta G_{\mathrm{int}}(T) \quad (17)$$

where $\Delta G_{\mathrm{Ubq-UIM}}(T)$, $\Delta G_{\mathrm{Ubq}}(T)$, $\Delta G_{\mathrm{UIM}}(T)$, and $\Delta G_{\mathrm{int}}(T)$ are the Gibbs energies of unfolding of Ubq−UIM, the Ubq core, the UIM helix, and the Ubq−UIM binding interface, respectively. In the context of this model, the unfolding cooperativity of Ubq−UIM can be conditionally described by the Gibbs energy of the Ubq−UIM binding interface relative to the Gibbs energies of the Ubq core and UIM helix. (a) If $\Delta G_{\mathrm{int}} \geq \Delta G_{\mathrm{Ubq}}$ and $\Delta G_{\mathrm{int}} \geq \Delta G_{\mathrm{UIM}}$, then Ubq−UIM will unfold cooperatively; (b) if $\Delta G_{\mathrm{int}} < \Delta G_{\mathrm{Ubq}}$ and/or $\Delta G_{\mathrm{int}} < \Delta G_{\mathrm{UIM}}$, then Ubq−UIM will unfold uncooperatively.

Four different substitutions were made to test the cooperativity of Ubq−UIM in the framework of this model.

(I) The H77V substitution replaces the His residue (conserved at this position) with Val. This substitution is known to increase Ubq−UIM binding affinity by a factor of 2 (*38*), and thus, H77V_Ubq−UIM would be expected to have a more stabilized interface between Ubq and UIM, i.e., larger ΔG_{int} than that in the Ubq−UIM construct. Furthermore, the H77V substitution is expected to stabilize the Ubq core (*82*) and thus would also cause an increase in ΔG_{Ubq}.

(II) The Ser residue (100% conserved) upon substitution in S104A decreases Ubq−UIM binding affinity (*36*) and would destabilize the Ubq−UIM binding interface (lower ΔG_{int}) in S104A_Ubq−UIM compared to that in Ubq−UIM. Furthermore, the serine to alanine substitution will also increase the stability of UIM [because alanine has a higher helix propensity that serine (*83*, *84*)] and thus increase ΔG_{UIM}.

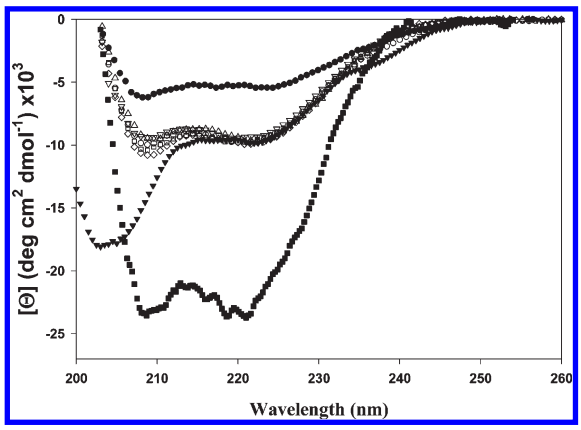

FIGURE 6: Far-UV circular dichroism spectra of the Ubq core (●), R98V_UIM peptide (▼), and all Ubq−UIM constructs: (○) Ubq−UIM1, (□) S104A_Ubq−UIM, (△) H77V_Ubq−UIM, (▽) E43N_Ubq−UIM, and (◇) R98V_Ubq−UIM. The difference spectrum between R98V_Ubq−UIM and Ubq calculated from eq 9 is shown as solid squares (■). For the sake of clarity, only every tenth data point is shown in all spectra.

(III) The E43N substitution at the C-cap position of the α-helix of Ubq is located on the opposite side from the UIM binding interface (Figure 1) and is known to destabilize the Ubq core (*85*). This variant (E43N_Ubq−UIM) would thus be expected to exhibit a ΔG_{Ubq} lower than that of the Ubq−UIM construct.

(IV) The R98V substitution is at a solvent-exposed position on the UIM helix that is not involved in the formation of the Ubq−UIM binding interface. Thus, the substitution of this arginine with a β-branched valine would destabilize the UIM helix (*83*, *84*), i.e., will lower the ΔG_{UIM} of R98V_Ubq−UIM.

All four variants, H77V_Ubq−UIM, E43N_Ubq−UIM, R98V_Ubq−UIM, and S104A_Ubq−UIM, show negligible differences in secondary structure content as evidenced from the comparison of the far-UV CD spectra to the spectrum of the Ubq−UIM construct (Figure 6). This suggests that there are no large conformational changes in these variants caused by the introduced substitutions. In addition, there is good agreement between the expected and observed changes in stabilities of the variants compared to that of Ubq−UIM. The H77V_Ubq−UIM variant is more thermostable than Ubq−UIM by ~7 °C, i.e., an increase in ΔG of unfolding of ~2 kJ/mol (see Table 1 and discussion below). This is consistent with the expected increase in both ΔG_{int} and ΔG_{Ubq}. The E43N substitution destabilizes the Ubq core by ~7 °C (*85*). The ~8 °C difference between the T_m values of Ubq−UIM and the E43N_Ubq−UIM variant (see Table 1 and discussion below) is in good agreement with the expected degree of destabilization based on the previous data (*85*). The R98V substitution significantly decreases the helical content of the R98V-UIM peptide, i.e., destabilizes the UIM helix [31% helical content at pH 7 and 25 °C (Figure 6)]. Despite this, the R98V_Ubq−UIM variant has the same far-UV CD spectrum as the other variants (Figure 6). This suggests that the degree of folding of the UIM helix in the R98V_Ubq−UIM variant is the same as for Ubq−UIM as evidenced by the similarity in the difference spectra between Ubq and Ubq−UIM and between Ubq and R98V_Ubq−UIM (see Figures 2 and 6). The decrease in the stability of the UIM helix in the R98V_Ubq−UIM variant is nevertheless reflected in a lower apparent thermodynamic stability for this variant (see Table 1 and discussion below).

Thermal unfolding profiles of Ubq−UIM, H77V_Ubq−UIM, E43N_Ubq−UIM, R98V_Ubq−UIM, and S104A_Ubq−UIM

monitored by near- and far-UV CD spectroscopy and by DSC are compared in Figures 5A, 5B, and 7, respectively. They reveal several interesting features that will be discussed below.

The unfolding profiles of H77V_Ubq−UIM and E43N_Ubq−UIM from DSC and far- and near-UV CD could be globally fitted to a two-state model (results in Table 1), using common thermodynamic parameters, T_m, $\Delta H(T_m)$, and ΔC_p, as described by eqs 10−12. This observation is consistent with the thermodynamic model described above and indicates that an increase in Ubq−UIM interface stability (higher ΔG_{int} as in H77V_Ubq−UIM) or changes in Ubq core stability (higher or lower ΔG_{Ubq}, in H77V_Ubq−UIM or E43N_Ubq−UIM, respectively) do not appear to disrupt the cooperativity observed in Ubq−UIM upon thermal unfolding.

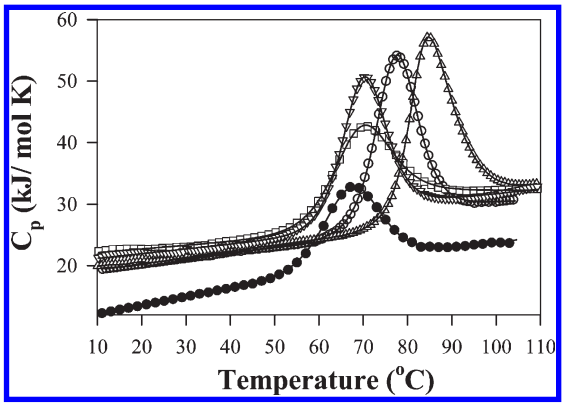

FIGURE 7: Temperature dependence of the partial molar heat capacity of the Ubq core and Ubq−UIM variants as monitored by DSC. Symbols show, for the sake of clarity, every third experimental data point: (●) ubiquitin core, (○) Ubq−UIM1, (□) S104A_Ubq−UIM, (△) H77V_Ubq−UIM, and (▽) E43N_Ubq−UIM. Solid lines represent the fit to a two-state model. The profile for R98V_Ubq−UIM could not be obtained because of the aggregation at the concentrations required for the DSC experiments.

The DSC-monitored melting profile for R98V_Ubq−UIM could not be obtained because of aggregation upon unfolding at the concentration required for a DSC experiment. However, the thermal melting profiles of this variant monitored by far- and near-UV CD also show a single sigmoidal transition (Figure 5A,B), and the data could be globally fitted to a two-state unfolding model (Table 1). This agreement between unfolding of R98V_Ubq−UIM at the secondary and tertiary structure levels indicates that unfolding cooperativity is retained in this variant. This is also consistent with the model, because the R98V substitution destabilizes the UIM helix (lower ΔG_{UIM}) without altering the Ubq−UIM interface stability; i.e., ΔG_{int} remains larger than ΔG_{UIM}.

The S104A_Ubq−UIM variant appears to be the most interesting. The far-UV CD melting profile does not appear to exhibit any sigmoidal shape (see Figure 5B), yet a noticeable sigmoidal shape is evident in the near-UV temperature-induced melting profile (Figure 5A). Moreover, the unfolding monitored by DSC clearly shows a heat absorption peak; however, this peak is much smaller than, for example, that of E43N_Ubq−UIM, which has approximately the same maximum temperature of partial heat capacity (see Figure 7). At first, one can assume that the UIM

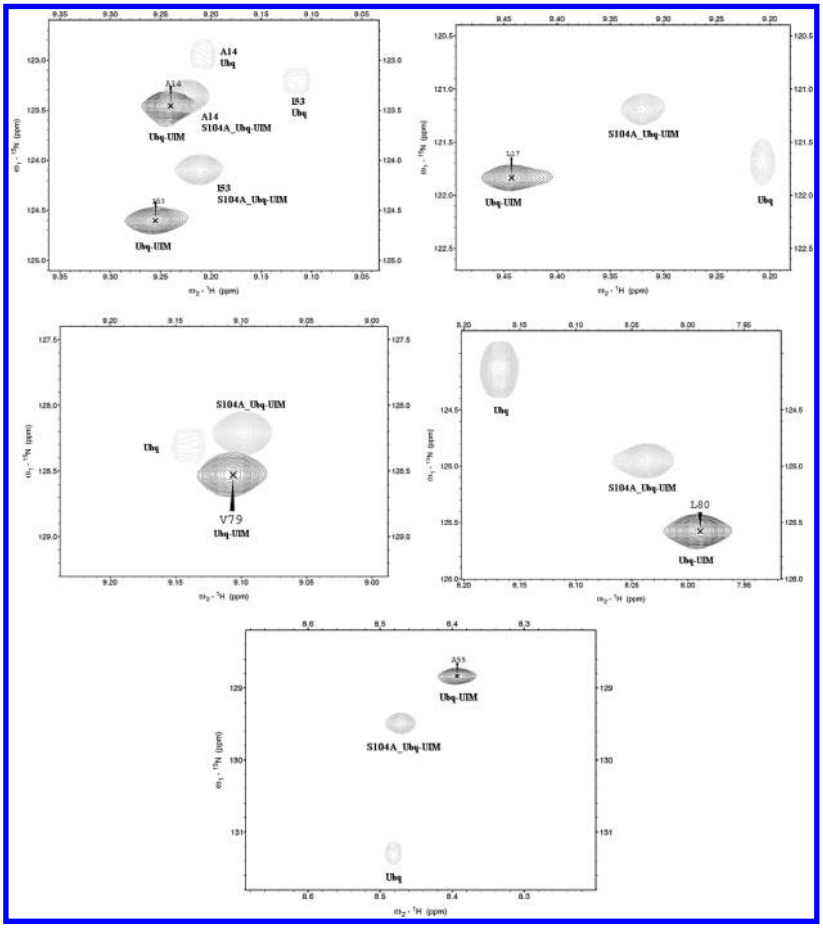

FIGURE 8: Expanded view of overlaid $^1H-^{15}N$ HSQC spectra of ubiquitin, the Ubq−UIM fusion protein, and the S104A_Ubq−UIM variant. Each panel shows representative key residues that were previously identified as being directly or indirectly involved in binding of the UIM helix to ubiquitin (*42*). For all residues, the chemical shifts of the S104A_Ubq−UIM variant appear at intermediate points between Ubq and Ubq−UIM.

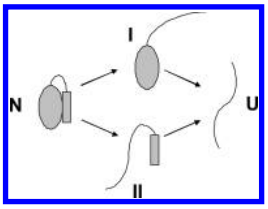

FIGURE 9: Thermodynamic model for the analysis of cooperativity in the Ubq−UIM system.

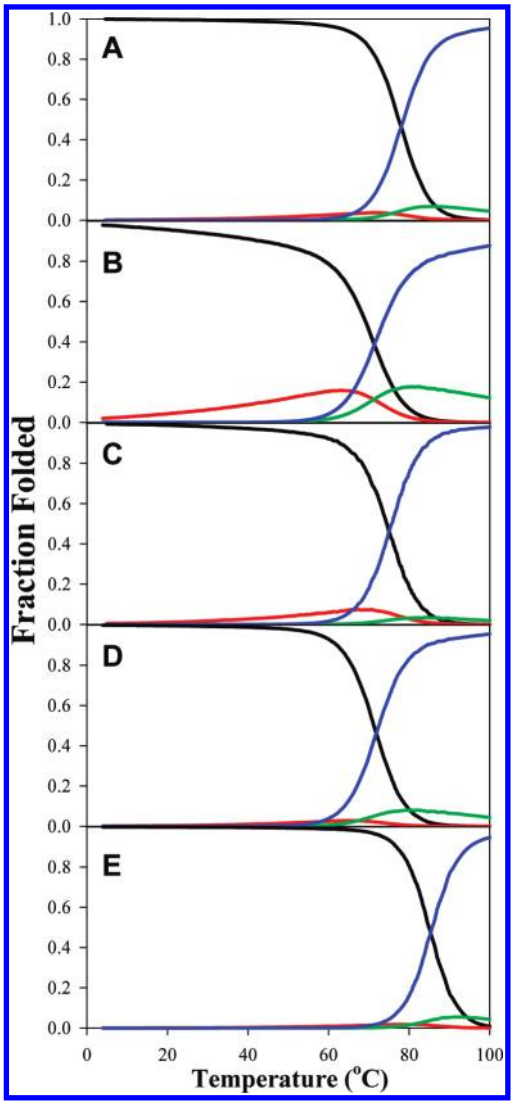

FIGURE 10: Temperature dependence of the populations of different states defined in Figure 9 and predicted using eqs 18−23: (A) Ubq−UIM, (B) S104A_Ubq−UIM, (C) R98V_Ubq−UIM, (D) E43N_Ubq−UIM, and (E) H77V_Ubq−UIM. Line colors correspond to the following states: N, black; I, red; II, green; U, blue.

helix in the S104A_Ubq−UIM variant does not dock onto the Ubq core. This is not the case as evidenced by the far-UV CD spectrum (see Figure 6) and by chemical shift positions in the HSQC spectrum (Figure 8) of S104A_Ubq−UIM. As discussed above, the far-UV CD spectrum of S104A_Ubq−UIM is very similar to those of other variants, suggesting similar structures. Also, the chemical shifts for the residues that have been previously identified by us (*42*) as forming the docking interface in the Ubq−UIM1 construct are also perturbed in the S104A_Ubq−UIM variant, albeit to a somewhat lower extent (Figure 8). This is probably a consequence of a weaker binding interface, as

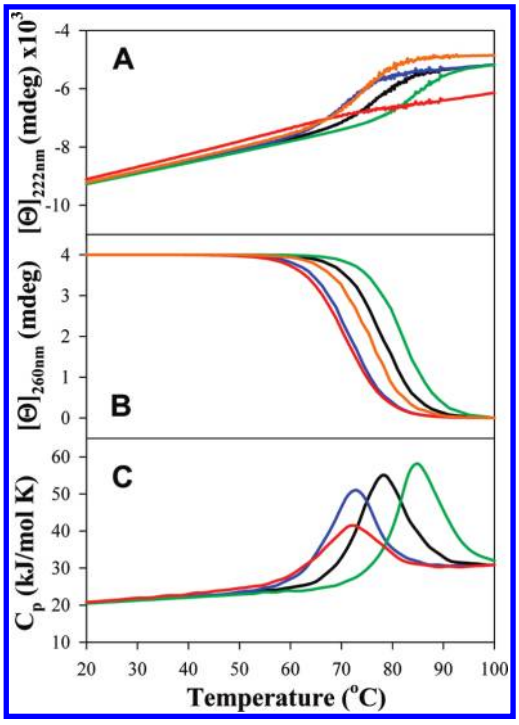

FIGURE 11: Predicted temperature dependence of the changes in the ellipticity in the far-UV CD at 222 nm (A), changes in the ellipticity in the near-UV CD at 260 nm (B), and changes in the partial molar heat capacity (C) for Ubq−UIM variants (Ubq−UIM, black; H77V_Ubq−UIM, green; S104A_Ubq−UIM, red; E43N_Ubq−UIM, blue; R98V_Ubq−UIM, orange). The profiles were computed on the basis of the populations of different states defined in Figure 10. Temperature dependencies of the CD profiles in panels A and B were calculated as $[\Theta] = \sum_i P_i[\Theta]_i$, where $[\Theta]$ is the molar ellipticity. The heat capacity profiles in panel C were calculated using a formalism previously outlined by Freire and Biltonen (*79*−*81*): $\langle \Delta C_{p,exc} \rangle = \sum_i \Delta H_i (\partial / \partial T) P_i + \sum_i P_i \Delta C_{p,i}$, where $\langle \Delta C_{p,exc} \rangle$ is the excess heat capacity function, ΔH is the average enthalpy, and ΔC_p is the heat capacity change upon unfolding.

observed in the peptide binding assays (*36*), and/or changes in the exchange time scale. Combined, these data suggest that the structure of S104A_Ubq−UIM is not different from those of the other proteins. What about cooperativity of unfolding? The melting profiles obtained from the DSC and near-UV CD experiments can be globally fit to a two-state unfolding model (see Table 1). However, both these methods report largely on the Ubq core and to a lesser degree on the unfolding of the UIM helix. Thus, to answer these questions, we turn to a more detailed thermodynamic model of protein cooperativity.

Thermodynamic Model of Cooperativity in Ubq−UIM. To put our experimental observation on a more quantitative thermodynamic foundation, we used the formalism developed by Freire (*78*−*81*). Figure 9 shows a schematic representation of the possible non-two-state unfolding mechanism of Ubq−UIM constructs. In this scheme, four different states can be realized: N-state, in which both Ubq and UIM are folded; intermediate I, which has the Ubq core folded and the UIM part unfolded; intermediate II, in which the UIM part is folded while the Ubq core is unfolded; and final U-state, in which both the Ubq core and UIM are unfolded. The partition function for this process will be a function of stabilities of individual domains, i.e., ΔG_{Ubq} for Ubq and ΔG_{UIM} for UIM, and of the stability of the interface between Ubq and UIM, ΔG_{int} (*78*):

$$Q = 1 + K_{Ubq}K_{int} + K_{UIM}K_{int} + K_{Ubq}K_{UIM}K_{int} \qquad (18)$$

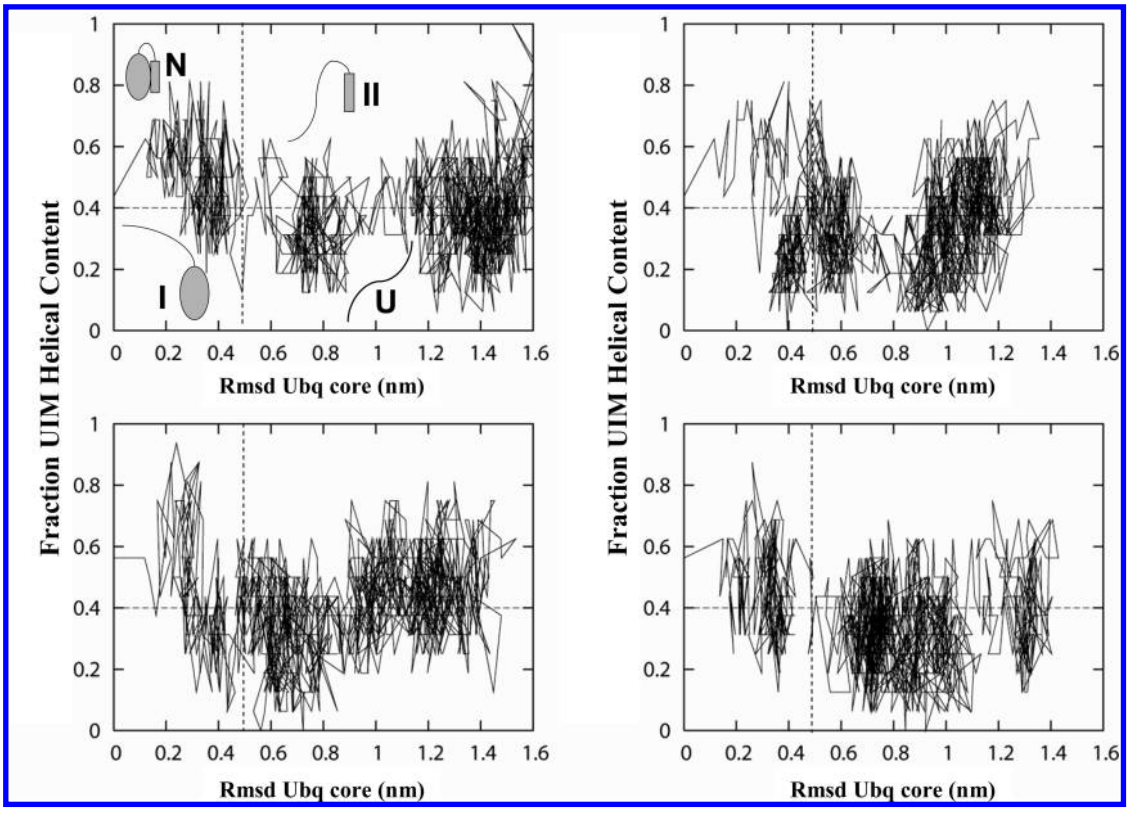

FIGURE 12: Representative molecular dynamics unfolding trajectories of Ubq−UIM. The figure shows four representative unfolding trajectories of Ubq−UIM as a function of the helical content fraction of the UIM helix and the rmsd of the Ubq core from the folded Ubq structure. The folded core corresponds to structures with an rmsd of approximately < 0.5 nm, and the unfolded UIM helix corresponds to helical fractions below 0.4 (although the distribution of helical content is not clearly bimodal). The four trajectories show that the system samples four states corresponding to the folded UIM−folded Ubq core (N), the unfolded UIM−folded Ubq core (I), the folded UIM−Ubq core (II), and the unfolded UIM−unfolded Ubq core (U). The top left frame shows cartoons of these four states as postulated by the thermodynamic model shown in Figure 9. Different trajectories follow different pathways among the four states. Given the nonequilibrium nature of the unfolding trajectories, we do not calculate the populations of the basins.

where the intrinsic equilibrium constants are defined as

$$K_{\mathrm{Ubq}} = \exp\left(\frac{-\Delta G_{\mathrm{Ubq}}}{RT}\right);$$

$$K_{\mathrm{UIM}} = \exp\left(\frac{-\Delta G_{\mathrm{UIM}}}{RT}\right); \text{ and } K_{\mathrm{int}} = \exp\left(\frac{-\Delta G_{\mathrm{int}}}{RT}\right) \quad (19)$$

The probability for each state, P_i, is then defined as

$$P_{\mathrm{N}} = \frac{1}{1 + K_{\mathrm{Ubq}}K_{\mathrm{int}} + K_{\mathrm{UIM}}K_{\mathrm{int}} + K_{\mathrm{Ubq}}K_{\mathrm{UIM}}K_{\mathrm{int}}} \quad (20)$$

$$P_{\mathrm{I}} = \frac{K_{\mathrm{UIM}}K_{\mathrm{int}}}{1 + K_{\mathrm{Ubq}}K_{\mathrm{int}} + K_{\mathrm{UIM}}K_{\mathrm{int}} + K_{\mathrm{Ubq}}K_{\mathrm{UIM}}K_{\mathrm{int}}} \quad (21)$$

$$P_{\mathrm{II}} = \frac{K_{\mathrm{Ubq}}K_{\mathrm{int}}}{1 + K_{\mathrm{Ubq}}K_{\mathrm{int}} + K_{\mathrm{UIM}}K_{\mathrm{int}} + K_{\mathrm{Ubq}}K_{\mathrm{UIM}}K_{\mathrm{int}}} \quad (22)$$

$$P_{\mathrm{U}} = \frac{K_{\mathrm{Ubq}}K_{\mathrm{UIM}}K_{\mathrm{int}}}{1 + K_{\mathrm{Ubq}}K_{\mathrm{int}} + K_{\mathrm{UIM}}K_{\mathrm{int}} + K_{\mathrm{Ubq}}K_{\mathrm{UIM}}K_{\mathrm{int}}} \quad (23)$$

Using this formalism, and using the thermodynamic parameters for stabilities of the Ubq core (Table 1) and UIM helix (see Figure S2 of the Supporting Information) as well as estimates for the energy of interactions (Table 1), we predicted populations of different states upon temperature-induced unfolding of all five variants: Ubq−UIM, H77V_Ubq−UIM, E43N_Ubq−UIM, R98V_Ubq−UIM, and S104A_Ubq−UIM. Figure 10 compares the probabilities of partially unfolded intermediates I and II with the probability of the N-state. The sum of probabilities for states I and II in Ubq−UIM at a given temperature never exceeds 8%, consistent with the experimental analysis that suggested that Ubq−UIM unfolding is very cooperative and close to two-state. Similar results are predicted for R98V_Ubq−UIM (9%), E43N_Ubq−UIM (9%), and H77V_Ubq−UIM (6%). This is dramatically different for S104A_Ubq−UIM, in which the sum of probabilities of intermediates I and II can be as high as 25%. To provide further support for this model, we calculated expected meting profiles for these proteins. Three panels in Figure 11 present the computed temperature-induced unfolding profiles expected for the near-UV CD, far-UV CD, and DSC experiments. The comparison with the experimental data is rather favorable: the model predicts rather well the transition temperatures, the changes in the enthalpy of unfolding, and also qualitatively the observed changes in the near-UV CD. In particular, the model predicts a lower enthalpy of unfolding of S104A_Ubq−UIM. The model also predicts rather gradual changes in the far-UV CD for the S104A_Ubq−UIM variant, and it also reproduces well the difference in the ellipticities of different constructs at high temperatures, which is a consequence of the difference in populations and intrinsic helical content of various UIMs: highest for S104A, lowest for R98V, and intermediate for UIM, which is common for Ubq−UIM, E43N_Ubq−UIM, and H77V_Ubq−UIM (Figure 11A).

Molecular Dynamics Simulations. Further support for the thermodynamic model of cooperativity comes from molecular dynamics (MD) simulations. To this end, we performed 100, 10 ns long, independent MD simulations at a high temperature (550 K) to simulate the unfolding of Ubq−UIM. These trajectories were analyzed to identify the population of states corresponding to the folded and unfolded states of the UIM helix and the Ubq core. In particular, we were interested in identifying states with the folded protein core and unfolded helix, and with the unfolded core and folded UIM helix, identified in the fitting of the thermodynamic equilibrium data. At this point of our work, we are not interested in studying the kinetics and unfolded transition states of the protein, which is usually done in unfolding simulations (*86*, *87*). We found that 99 of the 100 simulations unfolded during the 10 ns simulation time. The distribution of root-mean-square deviation (rmsd) distances from the folded state of the configurations sampled during all trajectories shows a clear separation of the folded and unfolded states with an rmsd of ~0.5 nm. The distribution, shown in Figure S3 of the Supporting Information, exhibit three peaks centered at 0.3 nm (assigned to the folded core) and 0.8 and 1.2 nm (assigned to the unfolded Ubq core). The fraction of UIM helical content shows a distribution that peaked at 0.4, 0.6, and 0.5 nm. Figure 12 shows four representative unfolding trajectories as a function of the UIM helical content and the Ubq core rmsd from the folded structures used to start the simulations. These trajectories clearly show that the Ubq−UIM system samples four states corresponding to the folded UIM−folded Ubq core, unfolded UIM−folded Ubq core, folded UIM−unfolded Ubq core, and unfolded UIM−unfolded Ubq core (states N, I, II, and U, respectively, in the thermodynamic model shown in Figure 9).

Concluding Remarks. Such close agreement between the thermodynamic model and experimental data with additional corroboration from the MD simulations provides strong support for the thermodynamic model of cooperativity. It also contains a cautionary note that one must be very careful when measuring the cooperativity of conformational transitions in proteins as some states are not highly populated and furthermore these conformational transitions can be masked by a relatively weak signal of certain experimental variables but not the others. For example, in the Ubq−UIM construct, species with Ubq unfolded and UIM folded are difficult to detect not only because their population is low but also because the enthalpy of helix unfolding is very low (*49*, *50*, *88*). This low enthalpy leads to very broad temperature-induced transitions and thus further limits its detection.

Overall, we have established the potential of the Ubq−UIM fusion construct in studying protein folding in terms of the relationship between isolated α-helices and those in larger or multidomain proteins. A logical continuation of this study is to investigate the folding kinetics of these fusion constructs to test whether Ubq, UIM, and/or interface stabilities can alter the energy landscape, and we are currently conducting experiments with this aim.

ACKNOWLEDGMENT

We thank Drs. Marimar Lopez (Rensselaer Polytechnic Institute) and Shigeyoshi Nakamura (Bruker) for designing and conducting the fluorescence anisotropy experiments to determine Ubq−UIM binding affinity, Dr. Scott McCallum (Rensselaer Polytechnic Institute) for help with NMR experiments, and Anne Stanley (The Pennsylvania State College of Medicine Macromolecular Core) for peptide synthesis. We acknowledge the use of the Core Facilities in the Center for Biotechnology and Interdisciplinary Studies, Rensselaer Polytechnic Institute.

SUPPORTING INFORMATION AVAILABLE

Sedimentation equilibrium profiles of Ubq and Ubq−UIM1−Ubq−UIM4, temperature dependence of the changes in ellipticity of UIM peptides, and rmsd distribution sampled in MD simulations. This material is available free of charge via the Internet at http://pubs.acs.org.

REFERENCES

1. Tan, Y. J., Oliveberg, M., and Fersht, A. R. (1996) Titration properties and thermodynamics of the transition state for folding: Comparison of two-state and multi-state folding pathways. *J. Mol. Biol. 264*, 377–389.
2. Ladurner, A. G., Itzhaki, L. S., de Prat Gay, G., and Fersht, A. R. (1997) Complementation of peptide fragments of the single domain protein chymotrypsin inhibitor 2. *J. Mol. Biol. 273*, 317–329.
3. Matouschek, A., Kellis, J. T., Jr., Serrano, L., Bycroft, M., and Fersht, A. R. (1990) Transient folding intermediates characterized by protein engineering. *Nature 346*, 440–445.
4. Jaenicke, R. (1999) Stability and folding of domain proteins. *Prog. Biophys. Mol. Biol. 71*, 155–241.
5. Privalov, P. L. (1982) Stability of proteins. Proteins which do not present a single cooperative system. *Adv. Protein Chem. 35*, 1–104.
6. Creighton, T. E. (1993) Proteins. Structures and Molecular Properties, 2nd ed., W. H. Freeman and Co., New York.
7. Fersht, A. R. (1997) Nucleation mechanisms in protein folding. *Curr. Opin. Struct. Biol. 7*, 3–9.
8. Conejero-Lara, F., Parrado, J., Azuaga, A. I., Smith, R. A., Ponting, C. P., and Dobson, C. M. (1996) Thermal stability of the three domains of streptokinase studied by circular dichroism and nuclear magnetic resonance. *Protein Sci. 5*, 2583–2591.
9. Inaba, K., Kobayashi, N., and Fersht, A. R. (2000) Conversion of two-state to multi-state folding kinetics on fusion of two protein foldons. *J. Mol. Biol. 302*, 219–233.
10. Cellitti, J., Llinas, M., Echols, N., Shank, E. A., Gillespie, B., Kwon, E., Crowder, S. M., Dahlquist, F. W., Alber, T., and Marqusee, S. (2007) Exploring subdomain cooperativity in T4 lysozyme I: Structural and energetic studies of a circular permutant and protein fragment. *Protein Sci. 16*, 842–851.
11. Jackson, S. E. (1998) How do small single-domain proteins fold? *Folding Des. 3*, R81–R91.
12. Krantz, B. A., Mayne, L., Rumbley, J., Englander, S. W., and Sosnick, T. R. (2002) Fast and slow intermediate accumulation and the initial barrier mechanism in protein folding. *J. Mol. Biol. 324*, 359–371.
13. Spudich, G. M., Miller, E. J., and Marqusee, S. (2004) Destabilization of the *Escherichia coli* RNase H kinetic intermediate: switching between a two-state and three-state folding mechanism. *J. Mol. Biol. 335*, 609–618.
14. Loh, S. N., Kay, M. S., and Baldwin, R. L. (1995) Structure and stability of a second molten globule intermediate in the apomyoglobin folding pathway. *Proc. Natl. Acad. Sci. U.S.A. 92*, 5446–5450.
15. Politou, A. S., Gautel, M., Improta, S., Vangelista, L., and Pastore, A. (1996) The elastic I-band region of titin is assembled in a "modular" fashion by weakly interacting Ig-like domains. *J. Mol. Biol. 255*, 604–616.
16. Scott, K. A., Steward, A., Fowler, S. B., and Clarke, J. (2002) Titin: A multidomain protein that behaves as the sum of its parts. *J. Mol. Biol. 315*, 819–829.
17. Cutler, T. A., and Loh, S. N. (2007) Thermodynamic analysis of an antagonistic folding-unfolding equilibrium between two protein domains. *J. Mol. Biol. 371*, 308–316.
18. Radley, T. L., Markowska, A. I., Bettinger, B. T., Ha, J. H., and Loh, S. N. (2003) Allosteric switching by mutually exclusive folding of protein domains. *J. Mol. Biol. 332*, 529–536.
19. Rudolph, R., Siebendritt, R., Nesslauer, G., Sharma, A. K., and Jaenicke, R. (1990) Folding of an all-β protein: Independent domain folding in γII-crystallin from calf eye lens. *Proc. Natl. Acad. Sci. U.S.A. 87*, 4625–4629.
20. Batey, S., and Clarke, J. (2006) Apparent cooperativity in the folding of multidomain proteins depends on the relative rates of folding of the constituent domains. *Proc. Natl. Acad. Sci. U.S.A. 103*, 18113–18118.

21. Peng, Z. Y., and Kim, P. S. (1994) A protein dissection study of a molten globule. *Biochemistry 33*, 2136–2141.
22. Wu, L. C., Grandori, R., and Carey, J. (1994) Autonomous subdomains in protein folding. *Protein Sci. 3*, 369–371.
23. Street, T. O., Bradley, C. M., and Barrick, D. (2007) Predicting coupling limits from an experimentally determined energy landscape. *Proc. Natl. Acad. Sci. U.S.A. 104*, 4907–4912.
24. Kloss, E., Courtemanche, N., and Barrick, D. (2008) Repeat-protein folding: New insights into origins of cooperativity, stability, and topology. *Arch. Biochem. Biophys. 469*, 83–99.
25. Billings, K. S., Best, R. B., Rutherford, T. J., and Clarke, J. (2008) Crosstalk between the protein surface and hydrophobic core in a core-swapped fibronectin type III domain. *J. Mol. Biol. 375*, 560–571.
26. Batey, S., Randles, L. G., Steward, A., and Clarke, J. (2005) Cooperative folding in a multi-domain protein. *J. Mol. Biol. 349*, 1045–1059.
27. Hofmann, K., and Falquet, L. (2001) A ubiquitin-interacting motif conserved in components of the proteasomal and lysosomal protein degradation systems. *Trends Biochem. Sci. 26*, 347–350.
28. Di Fiore, P. P., Polo, S., and Hofmann, K. (2003) When ubiquitin meets ubiquitin receptors: A signalling connection. *Nat. Rev. Mol. Cell Biol. 4*, 491–497.
29. Hicke, L., Schubert, H. L., and Hill, C. P. (2005) Ubiquitin-binding domains. *Nat. Rev. Mol. Cell Biol. 6*, 610–621.
30. Harper, J. W., and Schulman, B. A. (2006) Structural complexity in ubiquitin recognition. *Cell 124*, 1133–1136.
31. Hurley, J. H., Lee, S., and Prag, G. (2006) Ubiquitin-binding domains. *Biochem. J. 399*, 361–372.
32. Miller, S. L., Malotky, E., and O'Bryan, J. P. (2004) Analysis of the role of ubiquitin-interacting motifs in ubiquitin binding and ubiquitylation. *J. Biol. Chem. 279*, 33528–33537.
33. Hirano, S., Kawasaki, M., Ura, H., Kato, R., Raiborg, C., Stenmark, H., and Wakatsuki, S. (2006) Double-sided ubiquitin binding of Hrs-UIM in endosomal protein sorting. *Nat. Struct. Mol. Biol. 13*, 272–277.
34. Raiborg, C., Bache, K. G., Gillooly, D. J., Madshus, I. H., Stang, E., and Stenmark, H. (2002) Hrs sorts ubiquitinated proteins into clathrin-coated microdomains of early endosomes. *Nat. Cell Biol. 4*, 394–398.
35. Shekhtman, A., and Cowburn, D. (2002) A ubiquitin-interacting motif from Hrs binds to and occludes the ubiquitin surface necessary for polyubiquitination in monoubiquitinated proteins. *Biochem. Biophys. Res. Commun. 296*, 1222–1227.
36. Fisher, R. D., Wang, B., Alam, S. L., Higginson, D. S., Robinson, H., Sundquist, W. I., and Hill, C. P. (2003) Structure and ubiquitin binding of the ubiquitin-interacting motif. *J. Biol. Chem. 278*, 28976–28984.
37. Swanson, K. A., Kang, R. S., Stamenova, S. D., Hicke, L., and Radhakrishnan, I. (2003) Solution structure of Vps27 UIM-ubiquitin complex important for endosomal sorting and receptor downregulation. *EMBO J. 22*, 4597–4606.
38. Fujiwara, K., Tenno, T., Sugasawa, K., Jee, J. G., Ohki, I., Kojima, C., Tochio, H., Hiroaki, H., Hanaoka, F., and Shirakawa, M. (2004) Structure of the ubiquitin-interacting motif of S5a bound to the ubiquitin-like domain of HR23B. *J. Biol. Chem. 279*, 4760–4767.
39. Wang, Q., Young, P., and Walters, K. J. (2005) Structure of S5a bound to monoubiquitin provides a model for polyubiquitin recognition. *J. Mol. Biol. 348*, 727–739.
40. Haririnia, A., D'Onofrio, M., and Fushman, D. (2007) Mapping the interactions between Lys48 and Lys63-linked di-ubiquitins and a ubiquitin-interacting motif of S5a. *J. Mol. Biol. 368*, 753–766.
41. Bilodeau, P. S., Winistorfer, S. C., Kearney, W. R., Robertson, A. D., and Piper, R. C. (2003) Vps27-Hse1 and ESCRT-I complexes cooperate to increase efficiency of sorting ubiquitinated proteins at the endosome. *J. Cell Biol. 163*, 237–243.
42. Sgourakis, N. G., Patel, M. M., Garcia, A. E., Makhatadze, G. I., and McCallum, S. A. (2010) Conformational dynamics and structural plasticity play critical roles in the ubiquitin recognition of a UIM domain. *J. Mol. Biol. 396*, 1128–1144.
43. Ermolenko, D. N., Richardson, J. M., and Makhatadze, G. I. (2003) Noncharged amino acid residues at the solvent-exposed positions in the middle and at the C terminus of the α-helix have the same helical propensity. *Protein Sci. 12*, 1169–1176.
44. Khorasanizadeh, S., Peters, I. D., Butt, T. R., and Roder, H. (1993) Folding and stability of a tryptophan-containing mutant of ubiquitin. *Biochemistry 32*, 7054–7063.
45. Gribenko, A. V., Hopper, J. E., and Makhatadze, G. I. (2001) Molecular characterization and tissue distribution of a novel member of the S100 family of EF-hand proteins. *Biochemistry 40*, 15538–15548.
46. Pace, C. N., Vajdos, F., Fee, L., Grimsley, G., and Gray, T. (1995) How to measure and predict the molar absorption coefficient of a protein. *Protein Sci. 4*, 2411–2423.
47. Finn, R. D., Mistry, J., Schuster-Bockler, B., Griffiths-Jones, S., Hollich, V., Lassmann, T., Moxon, S., Marshall, M., Khanna, A., Durbin, R., Eddy, S. R., Sonnhammer, E. L., and Bateman, A. (2006) Pfam: Clans, web tools and services. *Nucleic Acids Res. 34*, D247–D251.
48. Makhatadze, G. I., Medvedkin, V. N., and Privalov, P. L. (1990) Partial molar volumes of polypeptides and their constituent groups in aqueous solution over a broad temperature range. *Biopolymers 30*, 1001–1010.
49. Richardson, J. M., and Makhatadze, G. I. (2004) Temperature dependence of the thermodynamics of helix-coil transition. *J. Mol. Biol. 335*, 1029–1037.
50. Richardson, J. M., McMahon, K. W., MacDonald, C. C., and Makhatadze, G. I. (1999) MEARA sequence repeat of human CstF-64 polyadenylation factor is helical in solution. A spectroscopic and calorimetric study. *Biochemistry 38*, 12869–12875.
51. Rohl, C. A., and Baldwin, R. L. (1998) Deciphering rules of helix stability in peptides. *Methods Enzymol. 295*, 1–26.
52. Brokx, R. D., Lopez, M. M., Vogel, H. J., and Makhatadze, G. I. (2001) Energetics of target peptide binding by calmodulin reveals different modes of binding. *J. Biol. Chem. 276*, 14083–14091.
53. Makhatadze, G. I., and Privalov, P. L. (1995) Energetics of protein structure. *Adv. Protein Chem. 47*, 307–425.
54. Ermolenko, D. N., Dangi, B., Gvritishvili, A., Gronenborn, A. M., and Makhatadze, G. I. (2007) Elimination of the C-cap in ubiquitin: Structure, dynamics and thermodynamic consequences. *Biophys. Chem. 126*, 25–35.
55. Berendsen, H. J. C., Postma, J. P. M., Vangunsteren, W. F., Dinola, A., and Haak, J. R. (1984) Molecular Dynamics with Coupling to an External Bath. *J. Chem. Phys. 81*, 3684–3690.
56. Parrinello, M., and Rahman, A. (1981) Polymorphic Transitions in Single Crystals: A New Molecular-Dynamics Method. *J. Appl. Phys. 52*, 7182–7190.
57. Nose, S. (1984) A Unified Formulation of the Constant Temperature Molecular-Dynamics Methods. *J. Chem. Phys. 81*, 511–519.
58. Hoover, W. G. (1985) Canonical Dynamics: Equilibrium Phase-Space Distributions. *Phys. Rev. A 31*, 1695–1697.
59. Hess, B., Bekker, H., Berendsen, H. J. C., and Fraaije, J. (1997) LINCS: A linear constraint solver for molecular simulations. *J. Comput. Chem. 18*, 1463–1472.
60. Miyamoto, S., and Kollman, P. A. (1992) Settle: An Analytical Version of the Shake and Rattle Algorithm for Rigid Water Models. *J. Comput. Chem. 13*, 952–962.
61. Hornak, V., Abel, R., Okur, A., Strockbine, B., Roitberg, A., and Simmerling, C. (2006) Comparison of multiple Amber force fields and development of improved protein backbone parameters. *Proteins 65*, 712–725.
62. Horn, H. W., Swope, W. C., Pitera, J. W., Madura, J. D., Dick, T. J., Hura, G. L., and Head-Gordon, T. (2004) Development of an improved four-site water model for biomolecular simulations: TIP4P-Ew. *J. Chem. Phys. 120*, 9665–9678.
63. Essmann, U., Perera, L., Berkowitz, M. L., Darden, T., Lee, H., and Pedersen, L. G. (1995) A Smooth Particle Mesh Ewald Method. *J. Chem. Phys. 103*, 8577–8593.
64. Van Der Spoel, D., Lindahl, E., Hess, B., Groenhof, G., Mark, A. E., and Berendsen, H. J. (2005) GROMACS: Fast, flexible, and free. *J. Comput. Chem. 26*, 1701–1718.
65. Byeon, I. J., Louis, J. M., and Gronenborn, A. M. (2004) A captured folding intermediate involved in dimerization and domain-swapping of GB1. *J. Mol. Biol. 340*, 615–625.
66. Predki, P. F., and Regan, L. (1995) Redesigning the topology of a four-helix-bundle protein: Monomeric Rop. *Biochemistry 34*, 9834–9839.
67. Robinson, C. R., and Sauer, R. T. (1996) Equilibrium stability and sub-millisecond refolding of a designed single-chain Arc repressor. *Biochemistry 35*, 13878–13884.
68. Nagi, A. D., and Regan, L. (1997) An inverse correlation between loop length and stability in a four-helix-bundle protein. *Folding Des. 2*, 67–75.
69. Chan, H. S., and Dill, K. A. (1989) Intrachain loops in polymers: Effects of excluded volume. *J. Chem. Phys. 90*, 492–509.
70. Tzul, F. O., and Bowler, B. E. (2010) Denatured states of low-complexity polypeptide sequences differ dramatically from those of foldable sequences. *Proc. Natl. Acad. Sci. U.S.A. 107*, 11364–11369.
71. Tamura, A., and Privalov, P. L. (1997) The entropy cost of protein association. *J. Mol. Biol. 273*, 1048–1060.

72. Yu, Y. B., Privalov, P. L., and Hodges, R. S. (2001) Contribution of translational and rotational motions to molecular association in aqueous solution. *Biophys. J. 81*, 1632–1642.
73. Ginsburg, A., and Carroll, W. R. (1965) Some Specific Ion Effects on the Conformation and Thermal Stability of Ribonuclease. *Biochemistry 4*, 2159–2174.
74. Lumry, R., Biltonen, R., and Brandts, J. F. (1966) Validity of the "two-state" hypothesis for conformational transitions of proteins. *Biopolymers 4*, 917–944.
75. Richardson, J. M., III, Lemaire, S. D., Jacquot, J. P., and Makhatadze, G. I. (2000) Difference in the mechanisms of the cold and heat induced unfolding of thioredoxin h from *Chlamydomonas reinhardtii*: Spectroscopic and calorimetric studies. *Biochemistry 39*, 11154–11162.
76. Streicher, W. W., and Makhatadze, G. I. (2007) Unfolding thermodynamics of Trp-cage, a 20 residue miniprotein, studied by differential scanning calorimetry and circular dichroism spectroscopy. *Biochemistry 46*, 2876–2880.
77. Streicher, W. W., and Makhatadze, G. I. (2006) Calorimetric evidence for a two-state unfolding of the β-hairpin peptide trpzip4. *J. Am. Chem. Soc. 128*, 30–31.
78. Murphy, K. P., and Freire, E. (1992) Thermodynamics of structural stability and cooperative folding behavior in proteins. *Adv. Protein Chem. 43*, 313–361.
79. Freire, E., and Biltonen, R. L. (1978) Statistical Mechanical Deconvolution of Thermal Transitions in Macromolecules. 1. Theory and Application to Homogeneous Systems. *Biopolymers 17*, 463–479.
80. Freire, E., and Biltonen, R. L. (1978) Statistical Mechanical Deconvolution of Thermal Transitions in Macromolecules. 2. General Treatment of Cooperative Phenomena. *Biopolymers 17*, 481–496.
81. Biltonen, R. L., and Freire, E. (1978) Thermodynamic characterization of conformational states of biological macromolecules using differential scanning calorimetry. *CRC Crit. Rev. Biochem. 5*, 85–124.
82. Loladze, V. V., Ibarra-Molero, B., Sanchez-Ruiz, J. M., and Makhatadze, G. I. (1999) Engineering a thermostable protein via optimization of charge-charge interactions on the protein surface. *Biochemistry 38*, 16419–16423.
83. Makhatadze, G. I. (2005) Thermodynamics of α-Helix Formation. *Adv. Protein Chem. 72*, 199–226.
84. Pace, C. N., and Scholtz, J. M. (1998) A helix propensity scale based on experimental studies of peptides and proteins. *Biophys. J. 75*, 422–427.
85. Ermolenko, D. N., Thomas, S. T., Aurora, R., Gronenborn, A. M., and Makhatadze, G. I. (2002) Hydrophobic interactions at the Ccap position of the C-capping motif of α-helices. *J. Mol. Biol. 322*, 123–135.
86. Day, R., Bennion, B. J., Ham, S., and Daggett, V. (2002) Increasing temperature accelerates protein unfolding without changing the pathway of unfolding. *J. Mol. Biol. 322*, 189–203.
87. Day, R., and Daggett, V. (2003) All-atom simulations of protein folding and unfolding. *Adv. Protein Chem. 66*, 373–403.
88. Richardson, J. M., Lopez, M. M., and Makhatadze, G. I. (2005) Enthalpy of helix-coil transition: Missing link in rationalizing the thermodynamics of helix-forming propensities of the amino acid residues. *Proc. Natl. Acad. Sci. U.S.A. 102*, 1413–1418.